2007-01-0732

Vehicle Linear and Rotational Acceleration, Velocity and Displacement during Staged Rollover Collisions

Orion P. Keifer, Wesley C. Richardson, Peter D. Layson, Bradley C. Reckamp, and Thomas C. Heilmann
Applications Engineering Group, Inc.

ABSTRACT

Four full scale vehicle rollover tests, about the roll axis (X-axis), were staged using a sled attached to a large truck. Each vehicle was fitted with a nine-accelerometer array that approximated the center of gravity and two single axis accelerometers attached to the roof adjacent to the A-pillar/roof junction. The acceleration data was retrieved for three tests; however, the data recorder malfunctioned on the remaining test. Data was collected at 1000 hertz and processed to determine the linear and rotational acceleration with respect to each of the three vehicle coordinate axes. Rollover video and scene data were also collected to correlate vehicle rollover motion with the accelerometer data.

INTRODUCTION

Full scale rollover tests have been conducted over many years. Much of the work has been performed using various test sleds. One of the most common is the Federal Motor Vehicle Safety Standard (FMVSS) 208 sled test, which is conducted in accordance with SAE J2114, for example the Malibu tests (Orlowski, et al., 1985 and Bahling, et al., 1990). The FMVSS 208 test sled ramp angle is 23º and the test is conducted using an initial speed of 30 miles per hour. The sled is decelerated to a stop in less than 3 feet and a deceleration rate of at least 20 g's for a minimum of 0.04 seconds.

The test procedure used for this work has a sled angle of 34º and a deceleration rate of approximately 0.6 g's; however, the tests required minimal apparatus that can be used for most vehicles and nearly any test surface. The test vehicles were instrumented to determine both the angular and linear acceleration, from which the angular and linear velocities and displacements could be determined.

METHODOLOGY

Vehicles

The test vehicles for the testing included the following:

Vehicle	VIN	Color
1989 Buick Park Avenue Ultra	1G4CU54C0K1668358	Gold
1994 Oldsmobile 88 Royale	1G3HN52L9R4818549	Blue
1997 Pontiac Grand Am	1G2NE52TXVC866133	White
1995 Mercury Tracer	3MASM10J9SR647656	Green

Table 1. Vehicle data.

Vehicle	Mass kg	Length m	Width m	SSF*
Buick	1462	5.00	1.83	1.44
Oldsmobile	1573	5.08	1.88	1.36
Pontiac	1307	4.75	1.73	1.34
Mercury	1095	4.34	1.70	1.37

Table 2. Vehicle data. * Static Stability Factor (half the track width divided by the center of gravity height).

Sled

The sled was manufactured using a utility trailer frame set side-ways. Two fixed axles were attached to the frame. Two ramps, one for the front and one for the rear axles, were welded in

place at an angle of approximately 34º (Figure 1). The designed ramp angle was determined using a first order approximation, neglecting suspension compliance, such that all test vehicles would: first, be stable while the sled was stopped or accelerating and second, roll off the sled when the pusher truck was heavily braking. Rollover occurs when the line of action of the force through the center of gravity of the vehicle is forward of the front lip of the sled. That occurs when the sum of three angles exceed 90°. The three angles are the sled ramp angle, the angle formed by the ground and a line passing through the vehicle center of gravity, with the apex at the center of the outboard tire, which is calculated using the Static Stability Factor (SSF) and the friction angle due to braking, shown on Figure 2. In this first order approximation, the braking deceleration required to cause the vehicle to roll was calcuated between 0.35 and 0.4 g's, depending on the test vehicle. The front bumper of the pusher truck was removed and brackets fabricated for this test were mounted on the frame members. The sled was then pinned to the frame brackets with two transverse pins, one for each side.

Figure 1. Photograph of the sled arrangement.

Instrumentation

A computer system was assembled to collect data, the details of which are in Appendix A. All data was collected with 12 bit resolution.

The monitored accelerometers included a nine-accelerometer array, as proposed by Padgaonkar, et al. (1975) and Mital and King (1979), including three mutually perpendicular channels on the center accelerometer and the two channels for each of the three legs.

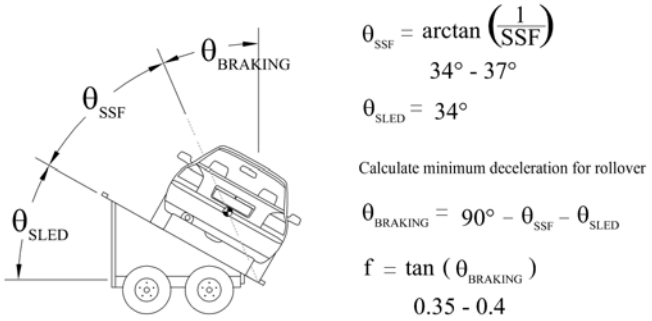

Figure 2. Diagram of the sled angles.

Three channels of a 2g triaxial accelerometer, installed on the floor near the center of gravity, were monitored. Two single axial 50g accelerometers were placed near the right and left A-pillar roof intersection. The position and orientation, with respect to the vehicle coordinate axis varied from vehicle to vehicle, but in general were oriented mostly vertically with a forward and outboard component as dictated by the interior contour at the A-pillar to roof contour inside the vehicle.

Additionally, one data collection channel monitored a microphone, used for video to data collection synchronization.

Figure 3 shows a photograph of the test equipment installed in one of the test vehicles.

Figure 3. Photograph of the nine-accelerometer array frame inside a test vehicle.

Video

Video cameras were used to capture the roll-over from the side and from the front. Cones were

placed on the test surface and measured as reference points for photogrammetric processing. The positions of the cones and video cameras were surveyed.

TEST PROCEDURE

The truck and sled were lined up on the test track and the vehicle was placed on the test sled. A balloon was popped adjacent to the test vehicle to provide synchronization between the data collection system and the video cameras. The video cameras captured the frame during which the balloons popped and the data recorder captured the sound on the channel which monitored the microphone.

The truck was accelerated and the speed of the truck was monitored with a Stalker radar gun. The truck steering was adequate to maintain a straight line of travel. As the truck crossed a predetermined line marked by cones, the driver locked up the brakes, causing the test vehicle to roll off the sled. When the vehicle came to final rest, a second balloon was popped adjacent to the final rest position of the vehicle, to synchronize the video with the data collection system. The data was downloaded from the data collection system via an Ethernet connection. The vehicle was photographed and marks on the pavement were documented.

RESULTS

The roll data and distance traveled is summarized in Table 3.

	Buick	Oldsmobile	Pontiac	Mercury
Lead direction	Driver	Passenger	Driver	Driver
Initial Vel. (kph)	55.5	54.7	56.3	56.3
Rolls*	2	2	4 1/4	1 1/2
Yaw (final rest)	10ºCW	70º CCW	35ºCW	20ºCW
Distance to Rest (m)	26.1	23.5	39.6	28.1
Drag factor	0.50	0.54	0.34	0.48

Table 3. Roll and distance data for the tested vehicles.
* Including the initial 34°.

Figures 4 through 7 show the damage received by the four vehicles during the rollover.

Figure 4. Buick

Figure 5. Oldsmobile

Figure 6. Pontiac

Figure 7. Mercury

Additional post-rollover photographs of the vehicles are enclosed in Appendix B. As defined by the authors, the roll of the vehicle began when the following side (upper ramp) tires first lifted off the ramp. The position of the test vehicle at tire lift-off was determined from video analysis and photogrammetry. The final rest position of the geometric center of the vehicle was determined by survey and checked using video analysis and photogrammetry. The initial speed of the test vehicle was determined by the peak speed from Stalker data. Of note, the peak speed was used from the Stalker data graphs for the Buick, Pontiac and Mercury. The graph for the Oldsmobile was not retained and therefore, the recorded peak speed was used.

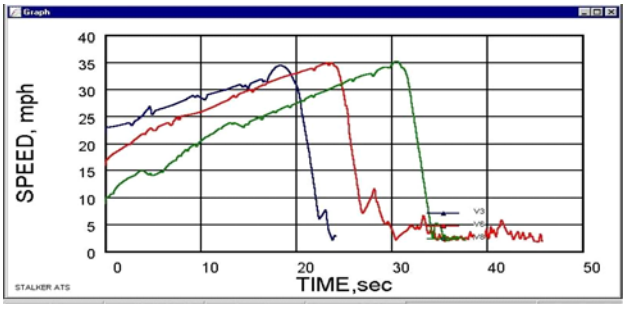

Figure 8. Stalker data. Left peak is for the Buick, middle peak for the Pontiac and the right peak is for the Mercury.

The distance traveled during the roll and the average drag factor was calculated and presented in Table 3.

Accelerometer Data Processing

Video and numerical data from the data collection system were first synchronized, and then the data of interest (approximately 15 seconds worth) was extracted.

The raw accelerometer data was processed by converting the voltage to multiples of the acceleration of gravity (g's) and applying corrections based on the calibration data for each accelerometer channel. The accelerometer offset was calculated and removed, based on the initial rest position where all acceleration data would correspond to the gravity vector. The data was then filtered using a digital four-pole Butterworth filter at 100 Hz. The filter used was SimFil, obtained from the NHTSA website, which meets the filtering requirements of SAE Surface Vehicle Recommended Practice J211-1 (SAE J211-1) for Channel Frequency Classes CFC-60 and CFC-180. It should be noted that the filtering frequency was the highest justified by the response of the accelerometers used. While it is less than the CFC-180 recommended for integration for speed and position, it exceeds the recommendation of CFC-60 for vehicle structural accelerations. Rotational acceleration was calculated using the formulation of Mital and King (1979). The rotational vectors were then transformed into the standard SAE vehicle coordinate system (positive x direction, forward, positive y direction to right and positive z direction, down). The transformed rotational acceleration data showed a bias both before the roll started and after final rest, when the values should have been zero. Linear correction to the data during the period of rollover motion was made to the rotational acceleration, which was then numerically integrated to determine the rotational velocity. A similar bias was seen in the angular velocity data, which was removed by a linear correction. The corrected angular velocity data was numerically integrated a second time for the rotational displacement. The calculated rotational displacement was compared to visual observation at final rest to determine the error, thus checking the initial accelerometer accuracy as well as the required corrections and vector transformations.

Vehicle	Calculated Roll Displacement	Visual Roll Displacement	Percent Error
Buick	665º	686º	3%
Oldsmobile	785º	686º	14%
Pontiac	1490º	1496º	0%

Table 4. Calculated roll displacement (double integration of the rotational acceleration data) compared to the visual roll displacement.

Table 4 compares the rotational displacement calculated by the double integration to the visual displacement. As can be seen, the error after the subtraction of accelerometer data and subsequent double integration is acceptably small for the Buick and the Pontiac. The integration data for the Oldsmobile suggests that the actual rotational acceleration is somewhat higher than recorded.

The rotational acceleration data for the Buick, Oldsmobile and Pontiac are presented in Figure 9. Note that the horizontal axes are matched for the

three vehicles for comparison. Darker backround indicates ground contact of the vehicle, based on video analysis. Larger graphs are presented in Appendix C.

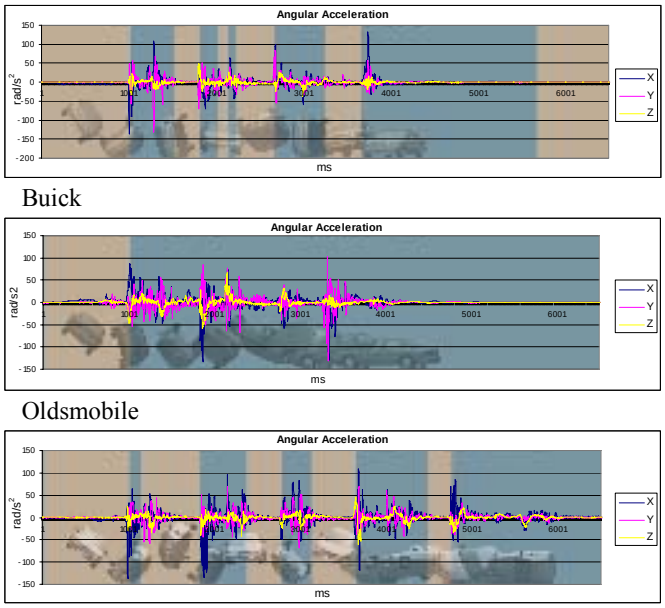

Figure 9. Triaxial angular acceleration for all three vehicles. Larger graphs are presented in Appendix C.

The X-axis rotational acceleration for the three vehicles is presented in Figure 10 and the X-axis rotational velocity for the three vehicles is presented in Figure 11. Note the darker background indicates that the vehicle is touching the ground and the light background, the vehicle is fully in the air, as determined by video analysis/photogrammetry. Clearly the ground contacts can be seen as linear and rotational acceleration spikes.

The linear acceleration was taken from the filtered acceleration data from the center tri-axial accelerometer and transformed into the vehicle coordinate axis. The linear acceleration is, however, confounded by the inclusion of gravity in the measured acceleration. To remove the effect of gravity, the position of the vehicle with respect to the ground reference was needed. Key frames of the synchronized videos were used to position a three dimensional computer model of the vehicle, with straight line motion calculated between key frames. The orientations of the model, every thousandth of a second, were calculated and the projection of the vehicle coordinate system on the ground z-vector was determined. These projections were subtracted from the accelerometer data.

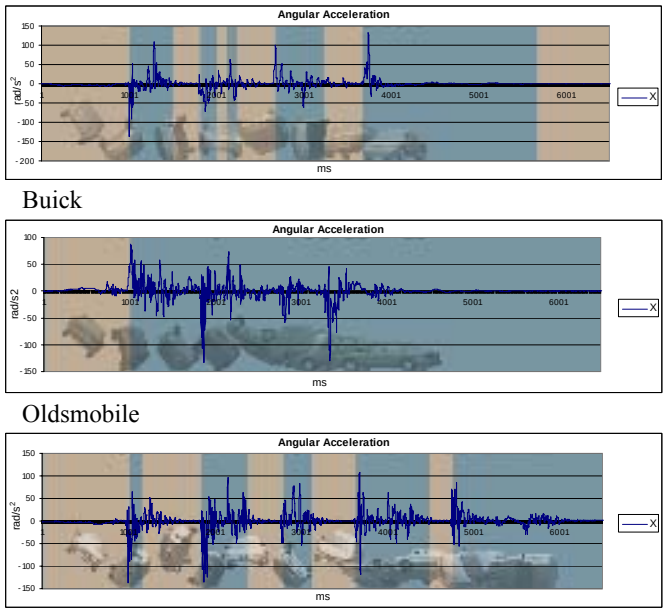

Figure 10. Rotational acceleration for X-axis for the three vehicles. Larger graphs are presented in Appendix C.

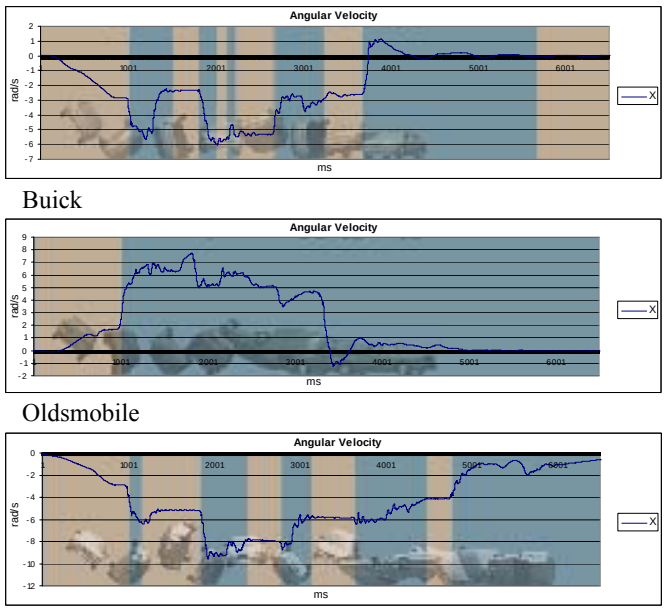

Figure 11. Angular velocity for all three vehicles. Larger graphs are presented in Appendix C.

The three axis linear acceleration data is presented for the three vehicles in Figure 12. The magnitude (vector sum) acceleration is presented in Figure 13.

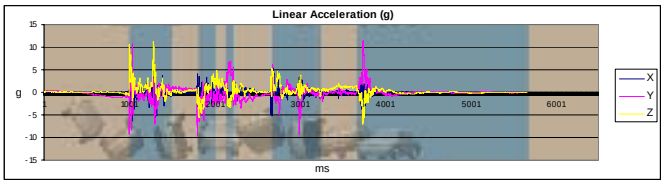

Buick

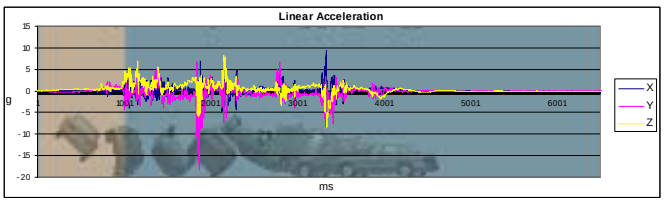

Oldsmobile

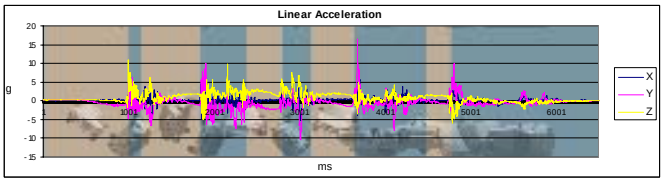

Pontiac

Figure 12. Triaxial linear acceleration of the three vehicles. Larger graphs are presented in Appendix C.

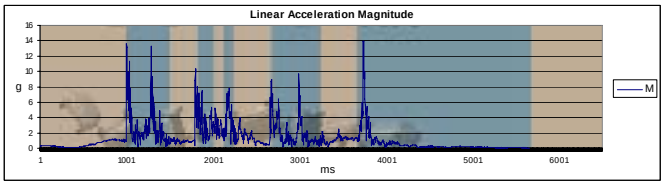

Buick

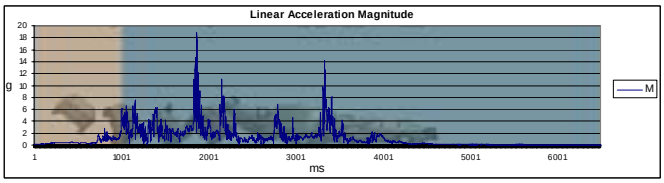

Oldsmobile

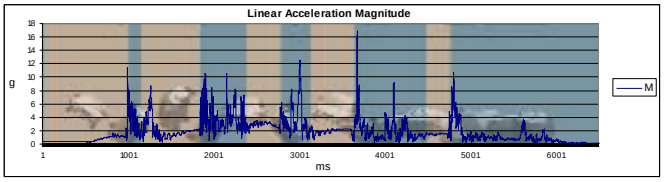

Pontiac

Figure 13. Magnitude (vector sum) of the linear acceleration of the three vehicles. Larger graphs are presented in Appendix C.

Single axis accelerometers were attached to the right and left A-pillars; however, the left A-pillar accelerometer failed. The data for the right A-pillar was converted from voltage to g's and filtered. Gravity was not, however, subtracted. The data is presented in Figure 14 for the three vehicles .

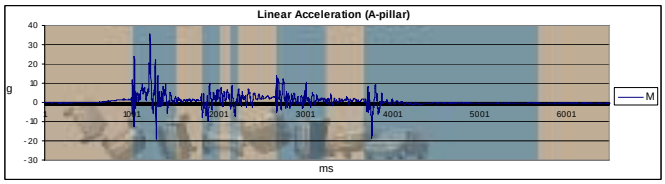

Buick

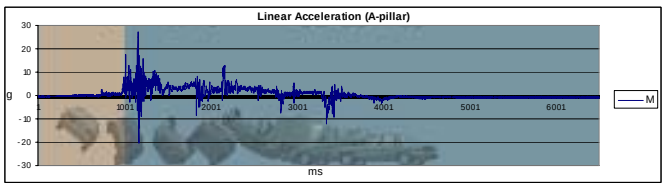

Oldsmobile

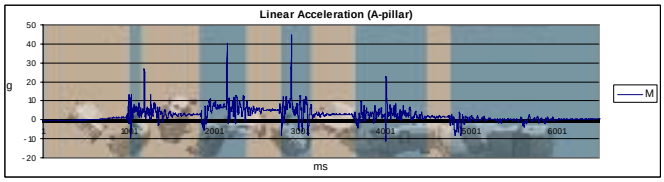

Pontiac

Figure 14. Left A-pillar accelerometer data. Larger graphs are presented in Appendix C.

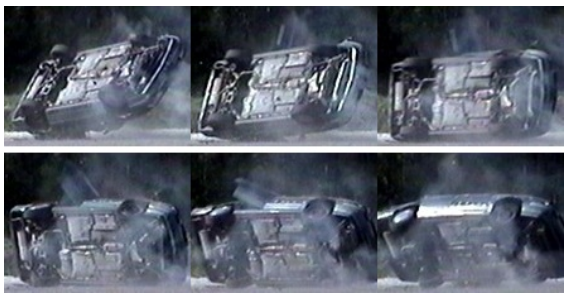

Figure 15. Oldsmobile test. Note the passenger side rear door opened and then shut (top rear in the video sequence above).

While reviewing the video, it was discovered that the passenger rear door on the Oldsmobile opened and then slammed shut during the roll sequence (Figure 15). At final rest, the door was latched shut.

DISCUSSION

While the test apparatus, test conditions and speed at which the vehicles were launched were similar, the resulting motion was significantly different, reflecting the chaotic nature of rollovers. This is consistent with the findings of Orlowski, et al. (1985) and Bahling, et al. (1990) and the observations of Moffatt, et al. (2003).

The average deceleration (effective drag) was calculated and ranged from 0.34 to 0.54. This

compares favorably with a range of 0.36 to 0.61 reported by Orlowski, et al. (1989). It should be noted that the distance used in calculating the effective drag in these tests is from lift-off of the following tires from the upper portion of the sled ramp to final rest. Further, the vehicle started at a position above the plane of the ground at a 34° angle from horizontal.

In these four tests, the Pontiac tended to impact the ground as the vehicle was coming up on its side, with the center of gravity more or less above the ground contact point. The principal direction of force therefore tended to pass near or behind the center of gravity and therefore the motion had a barrel roll appearance for the first 3+ rolls. This resulted in the most number of rolls (4¼) , the longest distance traveled (39.6m) and the lowest effective drag (0.34) for the four tests. During the final ¾ roll on the Pontiac, the vehicle yawed approximately 35º clockwise (CW) as seen from above resulting in a wheel down impact with the rear angled forward. That stopped most of the motion, except a slow roll onto its left (driver's) side. Interestingly, on the second ground impact, the rotational velocity for the Pontiac increased significantly from less than 5 to over 9 radians per second. At the end of the second roll, the anglular velocity was approximately 6 radians per second. It then slowed to approximately 4 radians per second until the wheel impact at the end of the fourth roll.

The Buick angular velocity barely reached 6 radians per second. At the end of the second roll, the vehicle landed relatively hard on its wheels, and the rotation was abruptly stopped. The Buick experienced a very slight approximately 10º clockwise CW yaw in the last ½ roll.

The Oldsmobile achieved an angular velocity of nearly 8 radians per second. During the last ½ roll, the vehicle yawed approximately 70º counter clockwise (CCW) and landed on its tires, with the rear forward, stopping the roll.

The Mercury motion was analyzed using video alone, because of the failure of the data collection system. The Mercury had what appeared to be a heavy impact after approximately 1 revolution which left tire rim gouges in the asphalt test surfaces and knocked off the hub caps. The first impact slowed the rotational velocity. The second impact was relatively flat on the roof which stopped the vehicles motion.

Review of the test data showed similar angular velocities as those reported by Orlowski, et al. (1985 and 1989).

The vehicles, as they approached their final rest, experienced a relatively flat (roof up or wheels up) impact to the forward edge, producing an upward force forward of the center of gravity. This resulted in a large retarding torque, effectively stopping the X-axis rotation. This can be seen in the angular velocity graphs shown in Appendix C. The stopping torque apeared quite large on the Oldsmobile and Buick, as compared to the impacts on the Pontiac. The vehicles in general showed some yaw during the last half roll, as recorded in Table 3.

Evidence of rollover impacts that are more side oriented, with the center of gravity above the impact and with multiple rolls, may suggest a lower effective drag coefficient during the roll phase as compared with a heavy forward edge flat impact with fewer rolls. This appears consistent with the Malibu tests, Orlowski, et al. (1985) and Bahling, et al. (1990), which also shows an inverse relationship between number of rolls and the average deceleration (effective drag coefficient), as shown in Table 5.

# rolls	# tests	Avg. distance (m)	Avg. drag
2	1	19.8	0.67
2 ½	2	21.35	0.63
3	4	23.63	0.57
3 ¼	2	26.8	0.50
3 ½	6	25.58	0.52
4	1	31.1	0.43

Table 5. Combined data for Malibu tests showing average deceleration (effective drag coefficient) appears inversely related to number of rolls.

The nine-accelerometer array was very effective in determining the rotational acceleration. The error in rotational displacement after normalizing the data and a double integration was 3 % or less for the Pontiac and Buick. The Oldsmobile, which showed the largest bias in the angular acceleration and velocity data, showed a displacement error on the order of 14%. The bias

corrections used in the angular accleration and velocity calculations were small compared to the peaks in the uncorrected data, well below that which can be detected on the graphical presentation of the data. The Oldsmobile was tested between the Buick and the Pontiac, with the test equipment moved from vehicle to vehicle. Therefore, test equipment malfunction is unlikely. It is important to note that the rotational acceleration is calculated by taking the difference between two accelerometer readings, which for low levels of angular acceleration can produce a large error as a percentage of the reading, while both of the original readings are within specifications. The percentage error is substantially reduced for higher differences. While the Oldsmobile had the greatest yaw during the final half revolution, it is not obvious why that would affect the roll integration which is taken about the X axis. While the source of the error could not be identified, it does not appear to be due to failure of any of the equipment and therefore it is likely to be relatively small error which spans the entire period of the roll. Therefore, the peak values are likely good indications of the peak rotational accelerations which the vehicle experienced.

It should be noted that angular rate (velocity) sensors are available and are typically used in rollover testing. In this testing, angular velocities of approximately 1½ rotations per second were seen, while many of the angular velocity sensors are linear to approximately 1 rotation per second. Further, rate sensors are not appropriate to determine impact rotational and linear accelerations. Rate sensors would be an excellent supplement to the 9-accelerometer array. Nonetheless, double integration of the rotational acceleration data should be performed as a check of the rotational acceleration data.

During the test of the Oldsmobile, its right rear door opened and closed. Prior to the beginning of the test, the door was latched but unlocked and at final rest the door was again latched. As can be seen in the photographs in Appendix B, the vehicle had experienced a lateral impact to the right rear quarter panel, but its relationship to the door opening, if any, is unknown.

The angular roll velocity achieved by the Buick and Oldsmobile was approximately one revolution per second. As mentioned earlier, the Pontiac's angular roll velocity was approximately 1½ revolutions per second after the second ground impact, but decreased to approximately 1 revolution per second after the third ground impact.

The magnitude of the linear acceleration for the vehicles achieved a peak of approximately 14 to 19 g's. These peaks were fairly narrow, approximately 10-20 ms.

Several areas can be improved in this test method. A rate sensor, to measure angular velocity is recommended in at least the X axis. Several video cameras, with fixed markers in the background would improve the precision of the video photogrammetry and would be useful in measuring the intitial speed of the vehicle as it begins to roll off the sled.

Rollovers by nature are chaotic. Therefore, in testing, as with actual rollover accidents, slight changes can produce significantly different results. This apparatus does not attempt to control all of the variables and therefore is not appropriate when repeatable results are to be achieved.

CONCLUSIONS

The rollover tests demonstrate the chaotic nature of rollover accidents and the difficulty in reconstruction. From this testing, as well as previous work that examines X-axis rolls on a flat surface, an increase in the number of rolls tends to result in greater travel distance and lower effective drag factor.

These tests demonstrate a simple, portable and inexpensive method of performing rollover tests with kinematic data. Additional video cameras, with known background markers and at least an X-axis rate sensor would improve the quality of the data collected.

ACKNOWLEDGMENTS

The authors wish to thank the Institute of Police Technology and Management, Mr. David Brill, who coordinated the testing in conjuction with the annual IPTM Special Problems Conference and Mr. Gary Stephens, who provided the truck and the financial support to construct the sled.

A special thank you to the AEGI staff, particularly Susan Stevens and Brenda Scruggs for their astute editing of this paper.

REFERENCES

Bahling, G.S., Bundorf, R.T., Kaspzyk, G.S., Moffatt, E.A., Orlowski, K.F., and Stocke, J.E., "Rollover and Drop Tests – The Influence of Roof Strength on Injury Mechanics Using Belted Dummies", SAE International, SAE Paper 902314, Warringdale, PA, 1990.

Mital, N.K., King, A.I., "Computation of Rigid-Body Rotation in Three-Dimensional Space from Body-Fixed Linear Acceleration Measurements", ASME, Journal of Biomechanical Engineering, 78-WA/Bio-5, American Society of Mechanical Engineers, 1978.

Moffatt, E.A., Cooper, E.R., Cronteau, J.J., Orlowski, K.F., Marth, D.R., and Carter, J.W., "Matched-Pair Rollover Impacts of Rollcaged and Production Roof Cars Using the Controlled Rollover Impact System (CRIS)", SAE paper 2003-01-0172, SAE International, Warrendale, PA, 2003.

Orlowski, K.F., Bundorf, R.F, and Moffatt, E.A., "Rollover Crash Tests – The Influence of Roof Strength on Injury Mechanics", SAE International, SAE Paper 851734, Warringdale, PA, 1985.

Orlowski, K.F., Moffatt, E.A. Bundorf, R.F, and Holcomb, M.P., "Reconstruction of Rollover Collisions", SAE International, SAE Paper 890857, Warringdale, PA, 1989.

Padgaonkar, A.J., Kreiger, K.W., and King, A.I., "Measurement of Angular Acceleration of a Rigid Body Using Linear Accelerometers", ASME, Journal of Applied Mechanics, 1975.

SAE J211-1 Recommended Practice "Instrumentation for Impact Test – Part 1 – Electronic Instrumentation", SAE International, Warringdale, PA.

SAE J2114 Recommended Practice "Dolly Rollover Recommended Test procedure", SAE International, Warringdale, PA.

CONTACT

Orion P. Keifer
Applications Engineering Group, Inc. (AEGI)
1200 Mayport Road
Atlantic Beach, Florida 32233
800-777-7668
opk@aegiforensics.com

Appendix A

INSTRUMENTATION

A computer system was assembled to collect data. The components included a VIA Motherboard 600MHz VIA C3 CPU, with integral ethernet, and 512 MB RAM, with a 12 volt power supply. The operating system was Windows 98 SE. Data was collected with a Data Translation 9800 USB A\D converter, using the included data software. Data was stored on a Sandisk Ultra 512 MB flash memory card. All data was collected with 12 bit resolution.

The accelerometers used are summarized in Table A-1. Power for the accelerometers was provided by a nine volt dry-cell battery through a five volt regulated power supply.

The monitored accelerometers included a nine-accelerometer array, as proposed by Padgaonkar, et al. (1975) and Mital and King (1979), including three mutually perpendicular channels on the center accelerometer and the two channels for each of the three legs. The leg accelerometers were triaxial, but only the two axes perpendicular to the axis of the leg were monitored, as shown in Figure A-1.

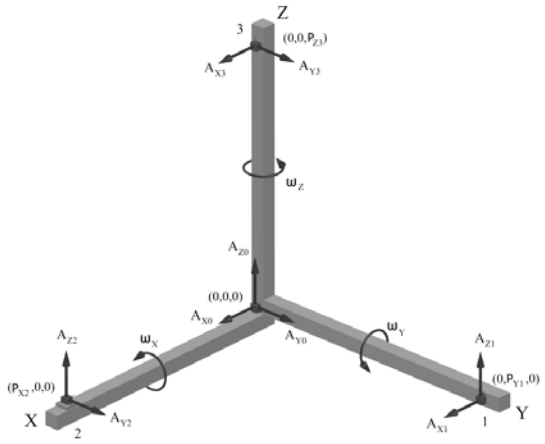

Figure A-1. Configuration of the nine-accelerometer array.

Linear acceleration in three directions are measured and used directly from the triaxial accelerometer at the origin of the array. Rotational accelerations are calculated by taking the difference between measured acceleration of two parallel accelerometer channels, divided by the perpendicular distance separating the accelerometer lines of action. As can be seen, angular acceleration about each of the axis can be calculated by using accelerometers on either of the other two axes. In this formulation, the two calculated angular accelerations are averaged. Mathematically from Mital and King (1979), equation 5:

$$\dot{\omega}_x = (A_{z1} - A_{z0})/2\rho_{y1} - (A_{y3} - A_{y0})/2\rho_{z3}$$

$$\dot{\omega}_y = (A_{x3} - A_{x0})/2\rho_{x3} - (A_{z2} - A_{z0})/2\rho_{x2}$$

$$\dot{\omega}_z = (A_{y2} - A_{y0})/2\rho_{x2} - (A_{x1} - A_{x0})/2\rho_{y1}$$

Where: $\dot{\omega}$ = angular acceleration
A = measured acceleration
ρ = distance between accelerometers (leg length)

Three channels of a 2g triaxial accelerometer, installed on the floor near the center of gravity, were monitored. Two single axial 50 g accelerometers were placed near the right and left A-pillar roof

intersection. The position and orientation, with respect to the vehicle coordinate axis varied from vehicle to vehicle, but in general were oriented mostly vertically with a forward and outboard component as dictated by the interior contour at the A-pillar to roof contour inside the vehicle.

Additionally, one data collection channel monitored a microphone, used for video to data collection synchronization and one channel monitored the five volt power supply for the accelerometers.

Position		Range	Manufact	Model	S/N
Array	Center	± 25 g's	Crossbow	CXL25LP3	0100927
	Leg 1	± 25 g's	Crossbow	CXL25LP3	0020972
	Leg 2	± 25 g's	Crossbow	CXL25LP3	0100926
	Leg 3	± 25 g's	Crossbow	CXL25LP3	9915614
CG fixed		± 2 g's	Crossbow	CXL02LP3	0019325
Left A Pillar		± 50 g's	Crossbow	CXL50LP3	0100054
Right A Pillar		± 50 g's	Crossbow	CXL50LP3	0023315

Table A-1. Accelerometer data and placement.

The nine-accelerometer array was attached to a steel frame with three mutually orthogonal legs. The frame was installed in the vehicles with the origin up as shown diagrammatically in Figure A-2.

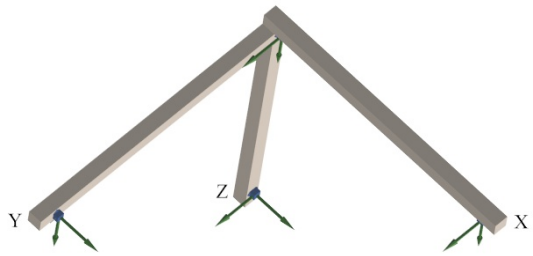

Figure A-2. Diagram of the nine-accelerometer array orientation in the test vehicles.

Appendix B

Buick Photographs

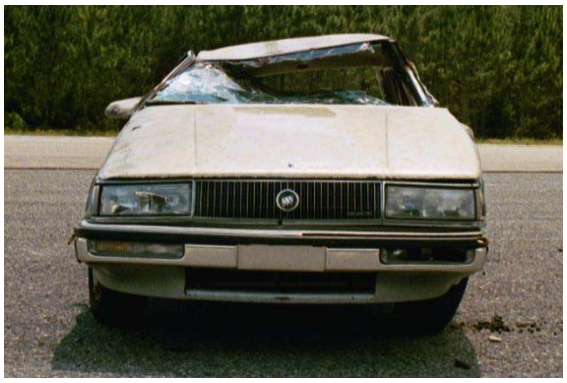

Figure B-1.

Figure B-2.

Figure B-3.

Figure B-4.

Figure B-5.

Figure B-6.

Appendix B

Oldsmobile Photographs

Figure B-7.

Figure B-8.

Figure B-9.

Figure B-10.

Figure B-11.

Figure B-12.

Appendix B

Pontiac Photographs

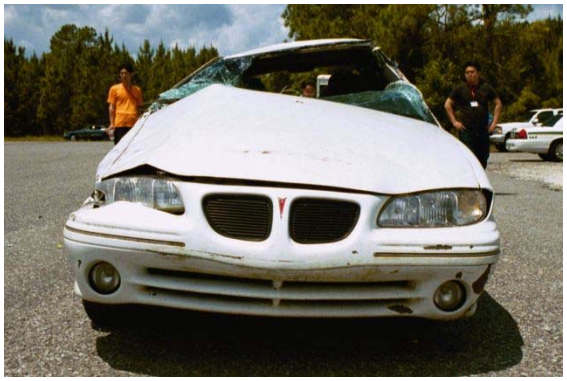

Figure B-13.

Figure B-14.

Figure B-15.

Figure B-16.

Figure B-17.

Figure B-18.

Appendix B

Mercury Photographs

Figure B-19.

Figure B-20.

Figure B-21.

Figure B-22.

Figure B-23.

Figure B-24.

Appendix C

Buick Accelerometer Data

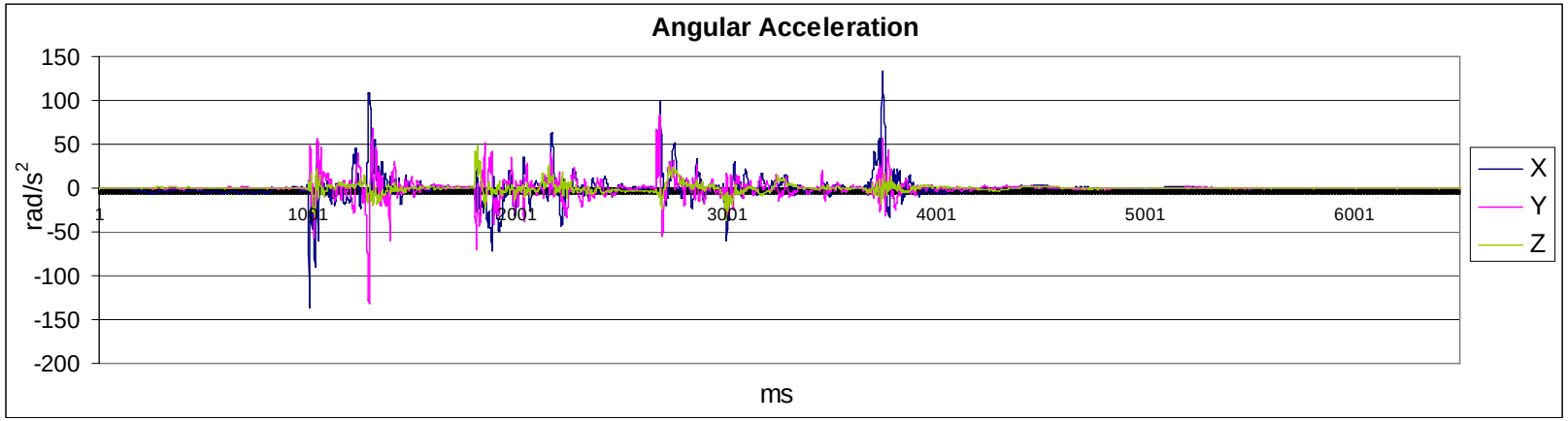

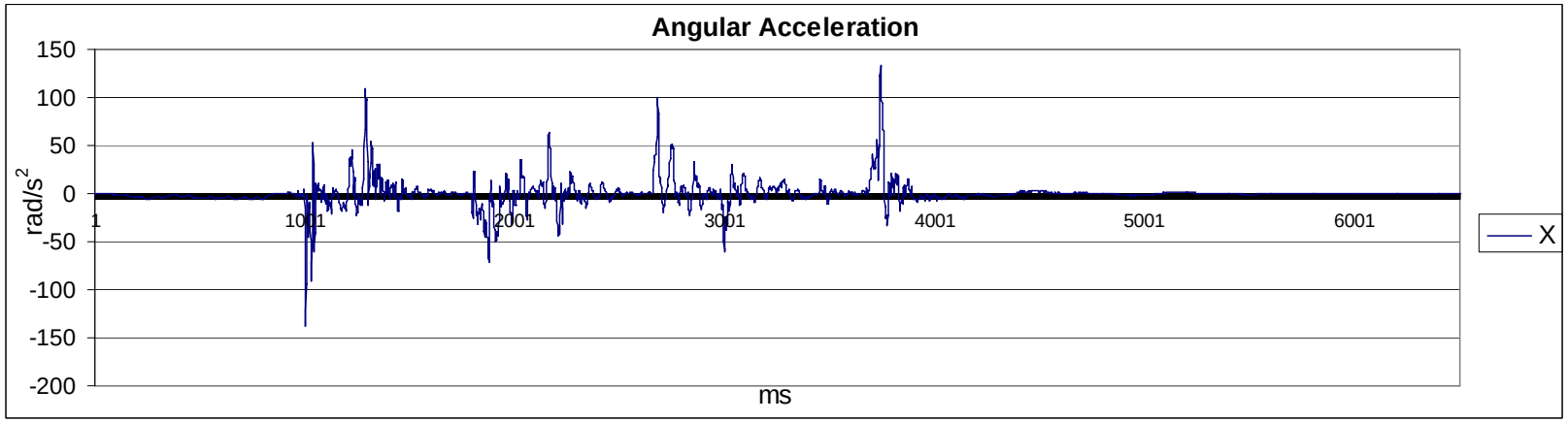

Appendix C

Buick Accelerometer Data

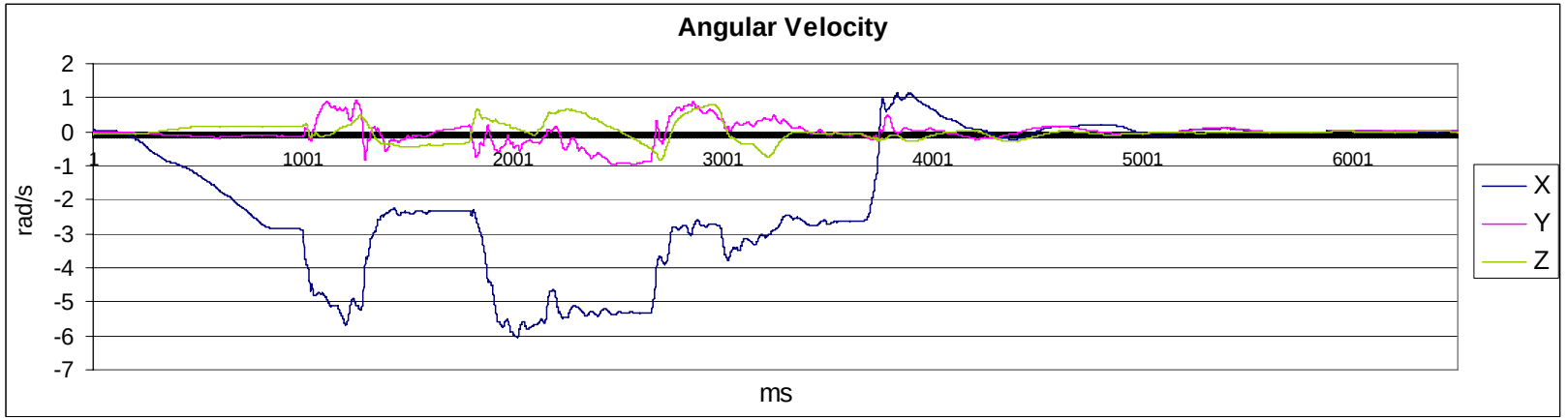

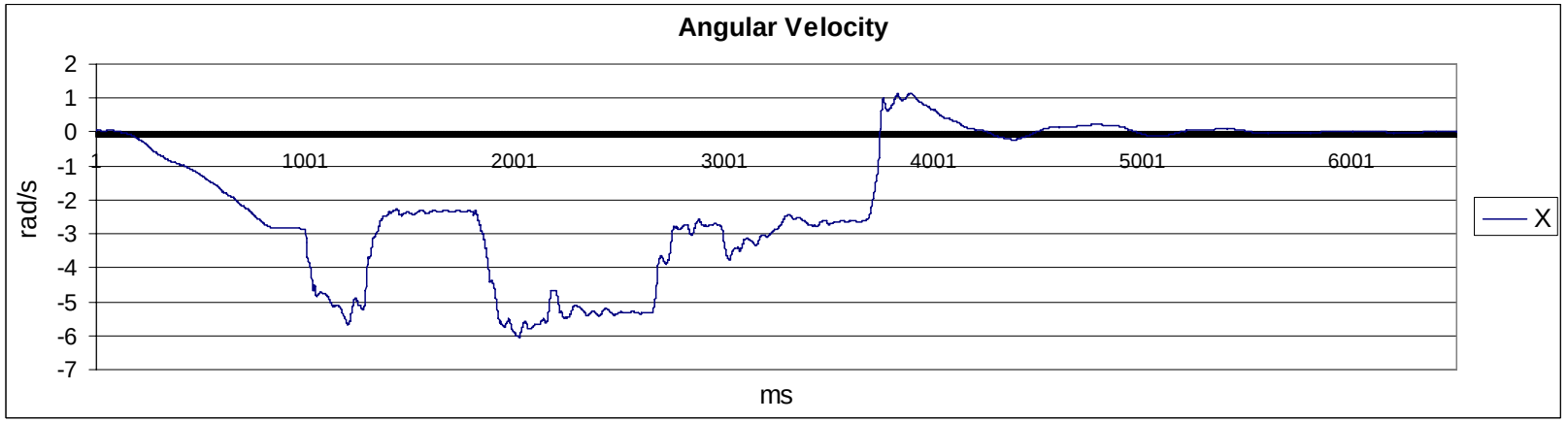

Appendix C

Buick Accelerometer Data

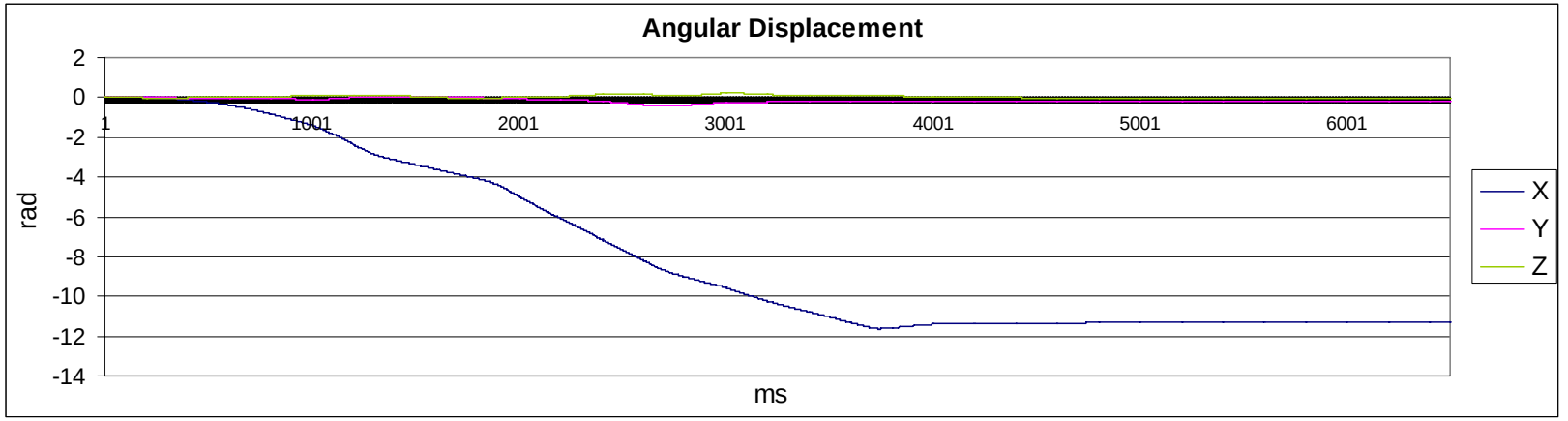

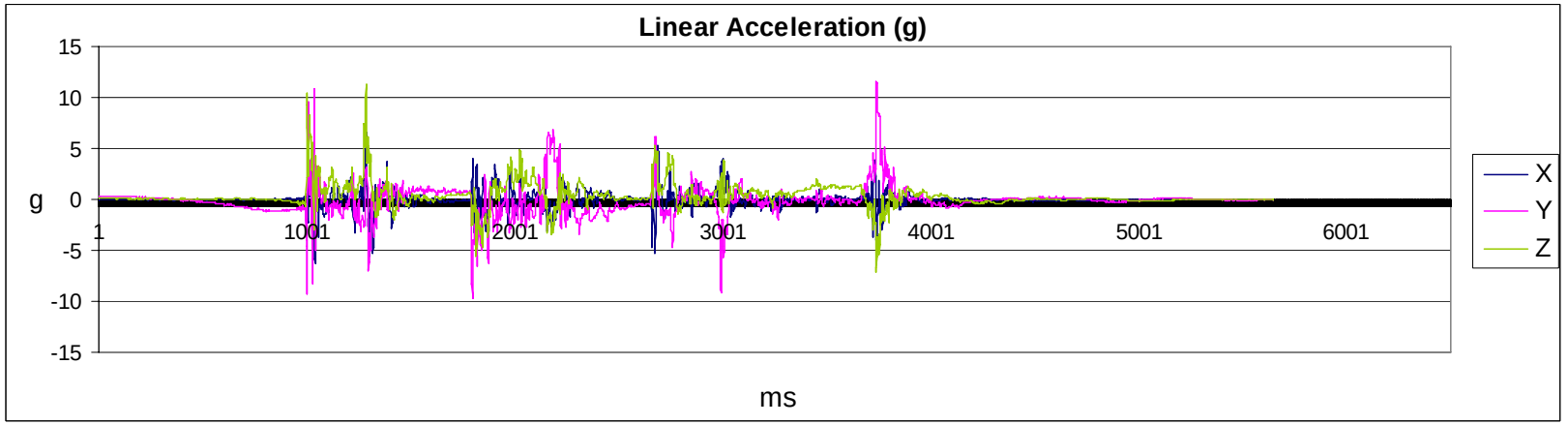

Appendix C

Buick Accelerometer Data

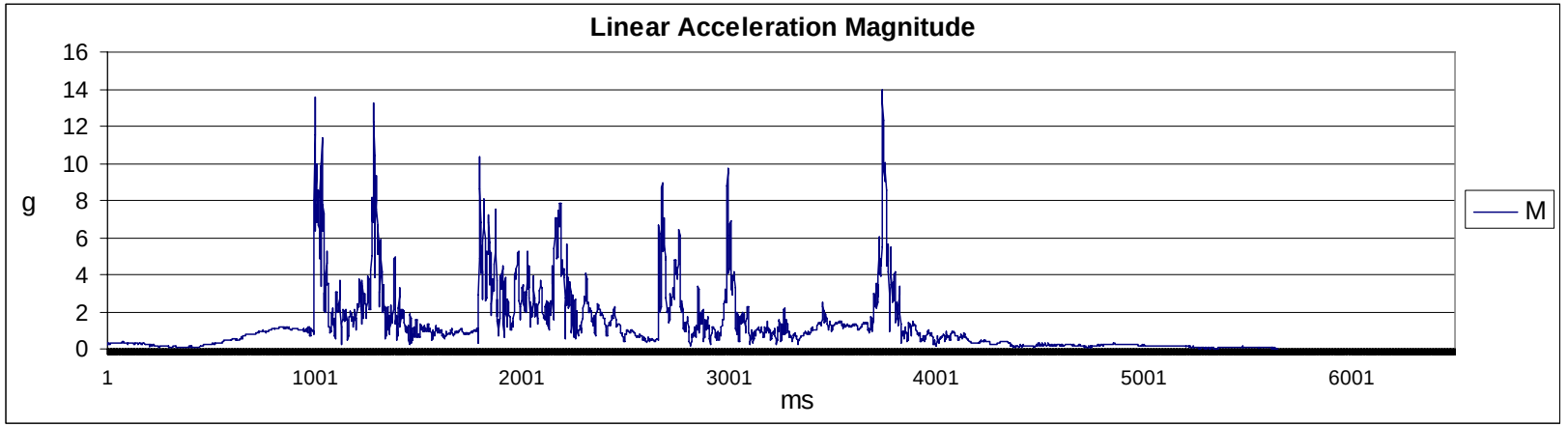

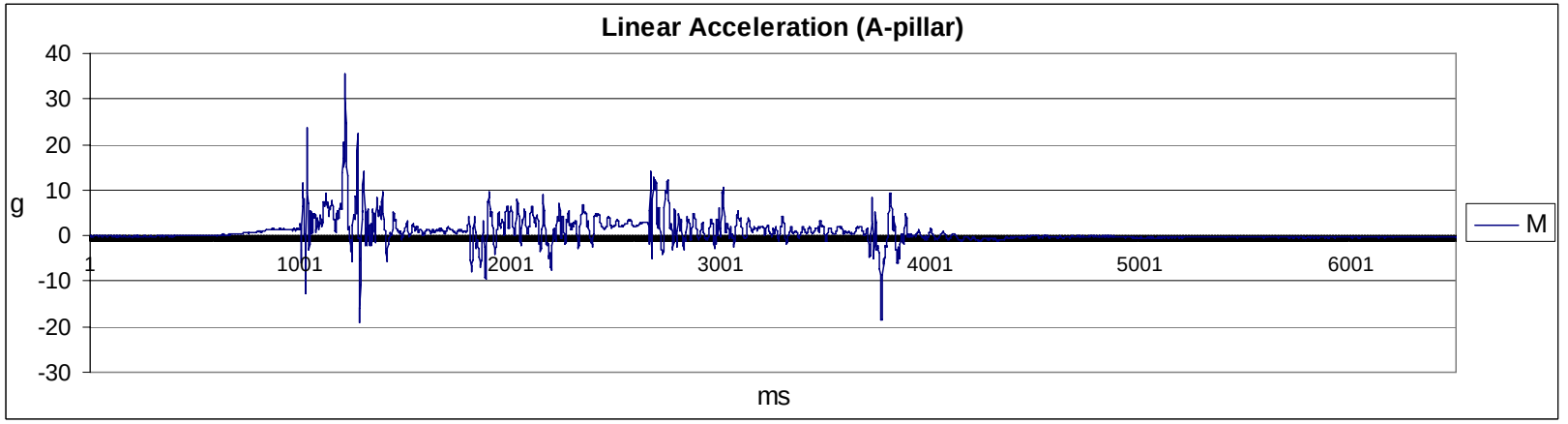

Appendix C

Oldsmobile Accelerometer Data

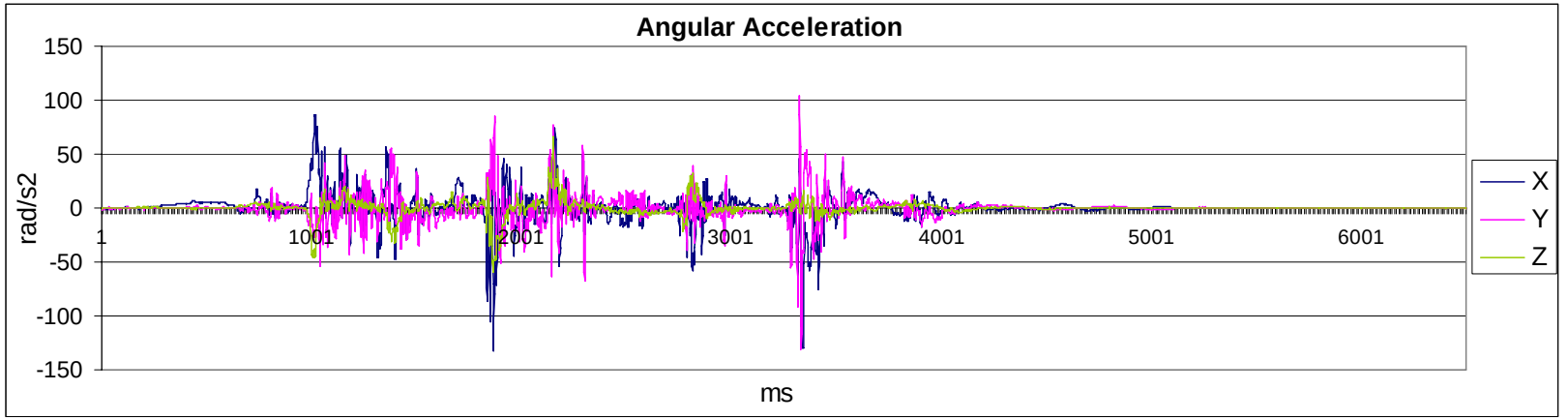

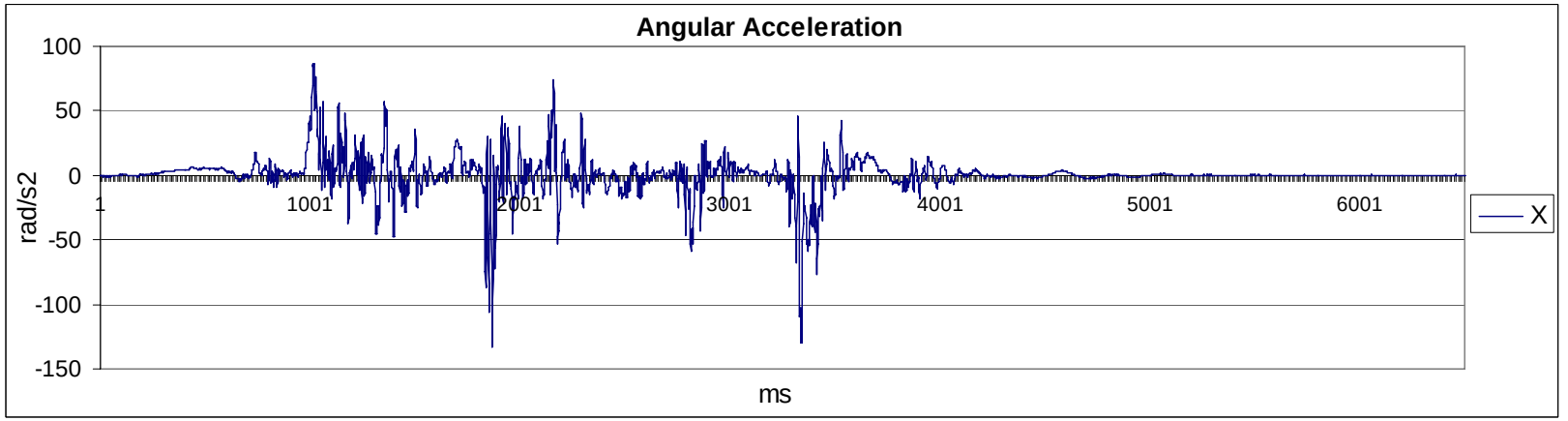

Appendix C

Oldsmobile Accelerometer Data

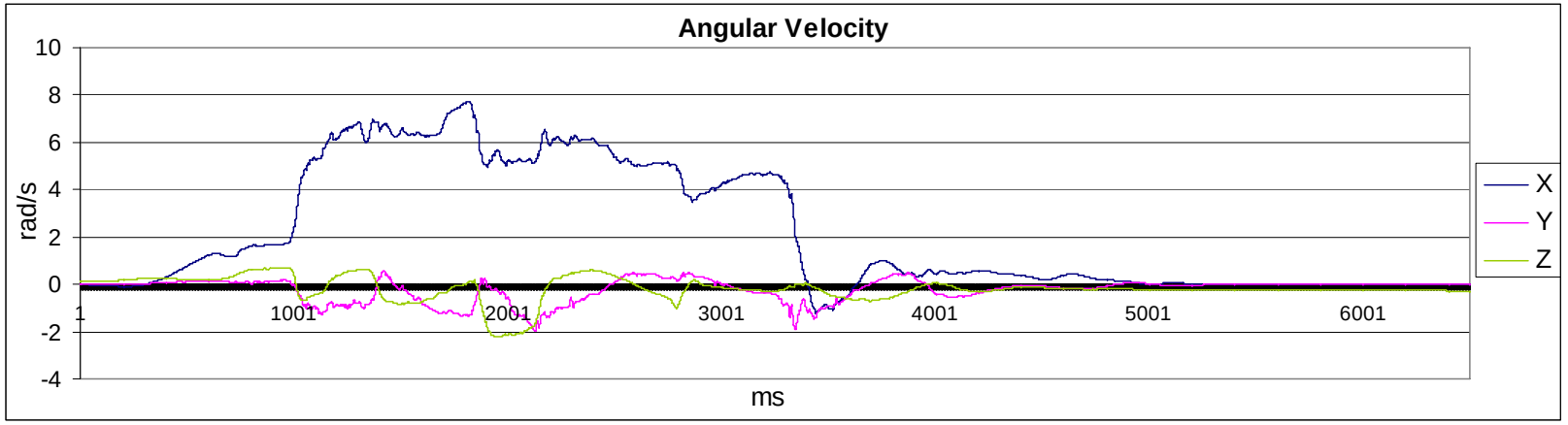

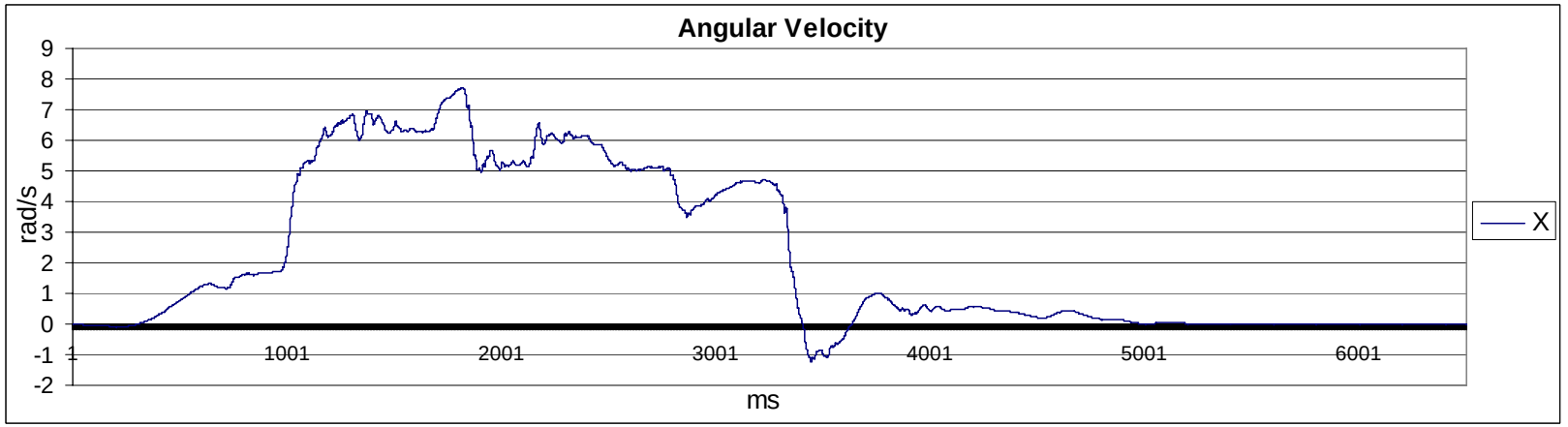

Appendix C

Oldsmobile Accelerometer Data

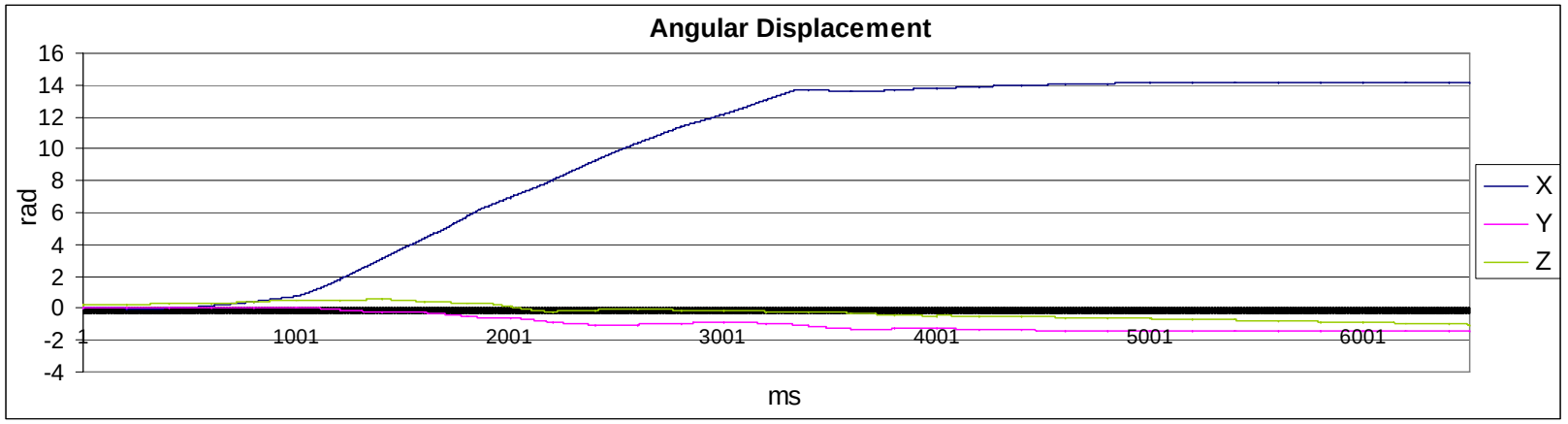

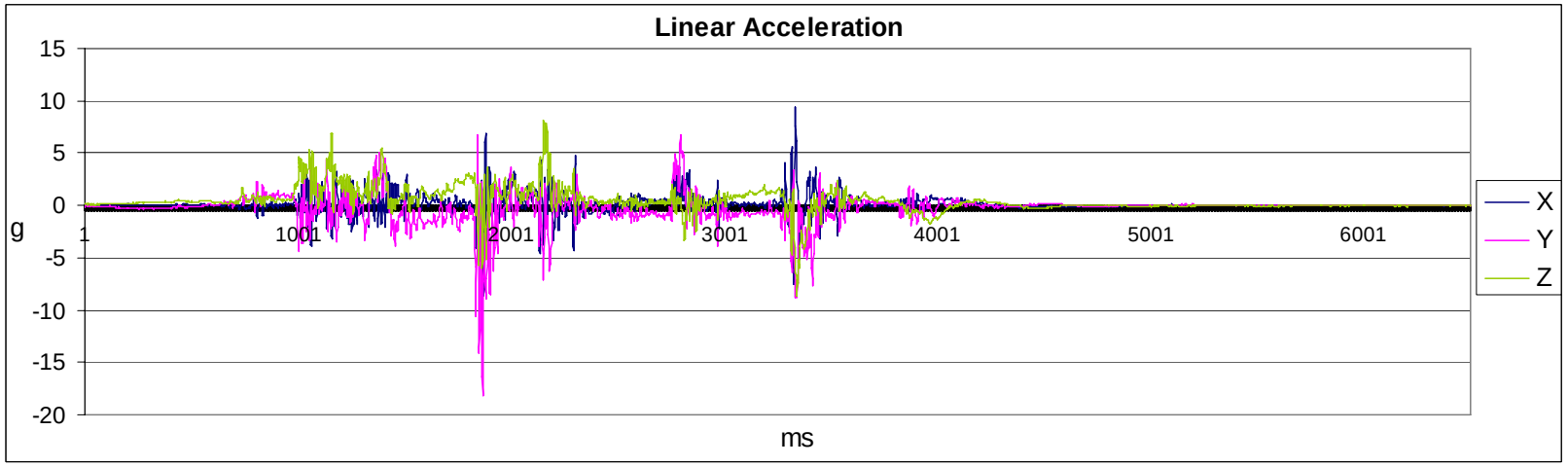

Appendix C

Oldsmobile Accelerometer Data

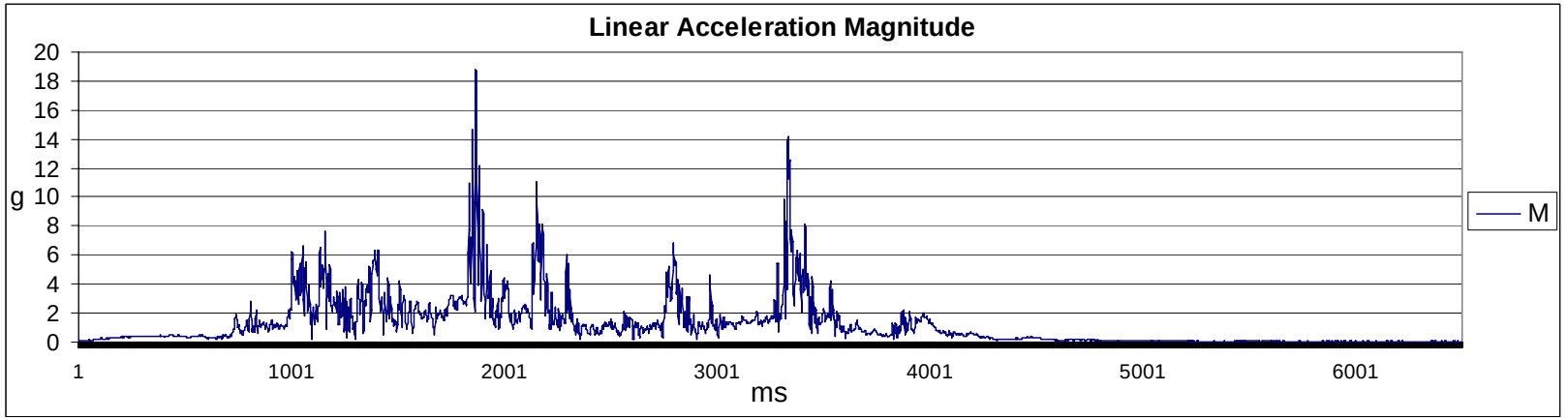

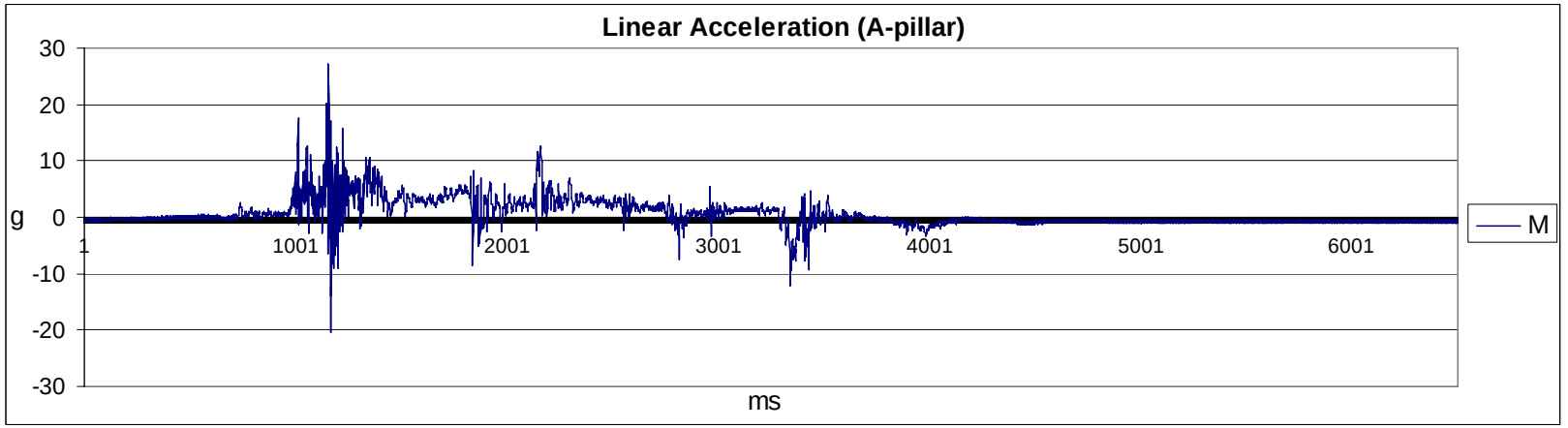

Appendix C

Pontiac Accelerometer Data

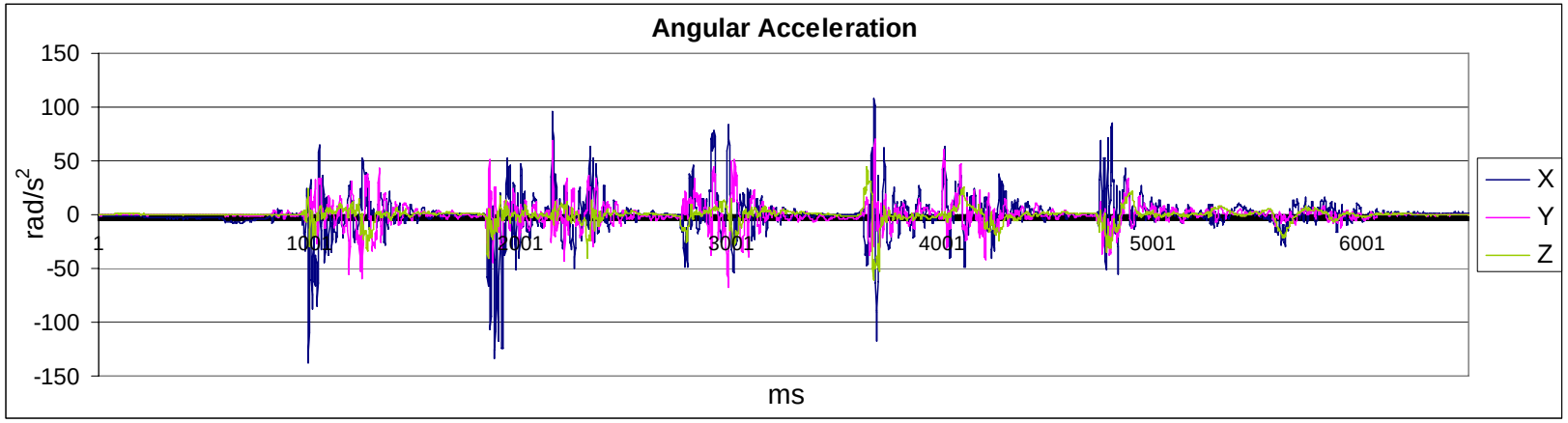

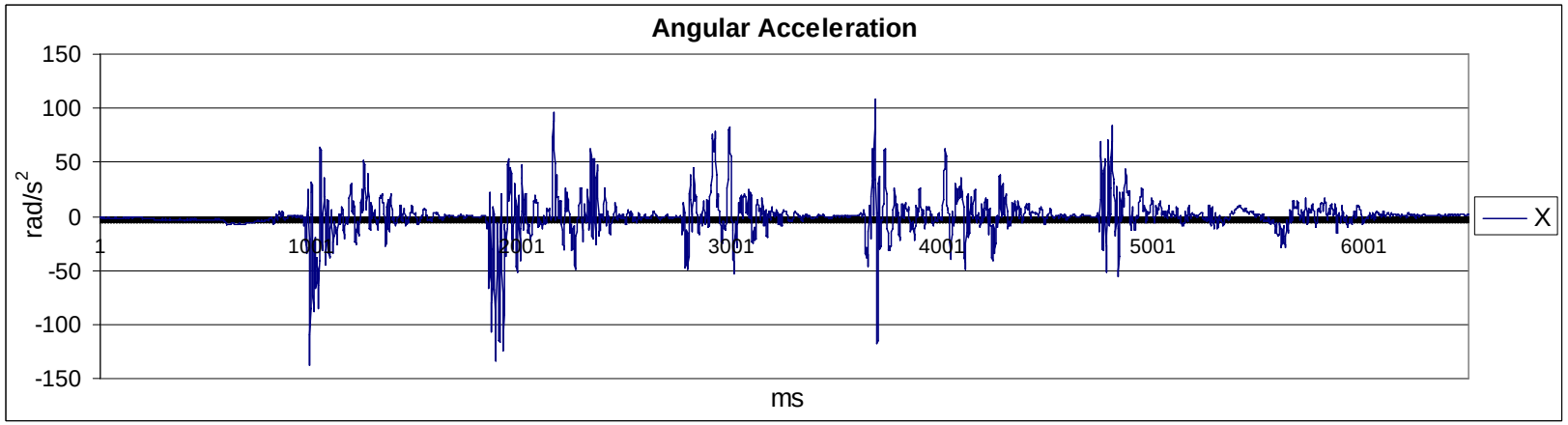

Appendix C

Pontiac Accelerometer Data

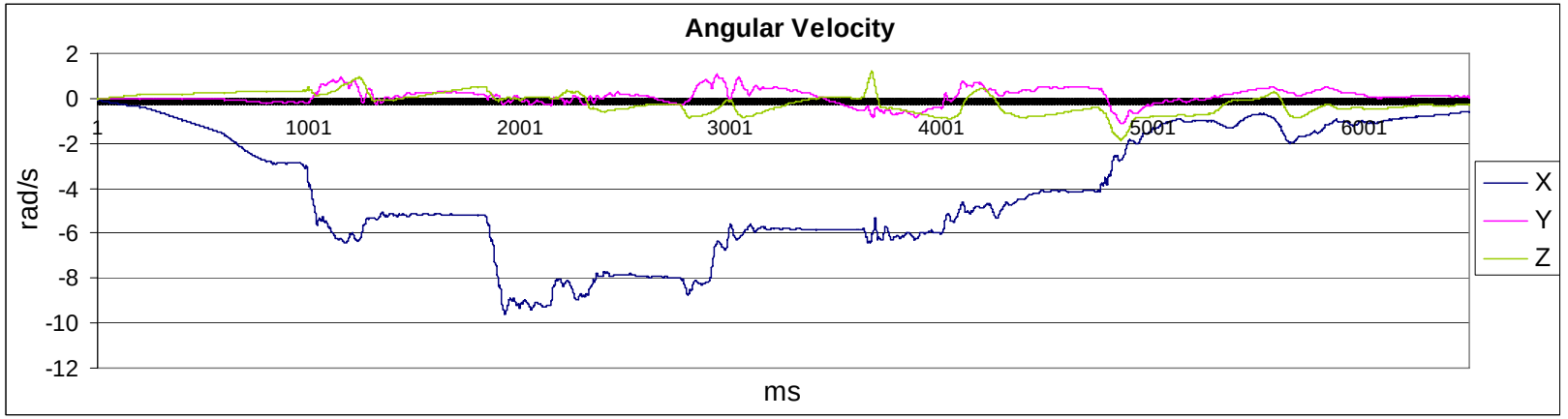

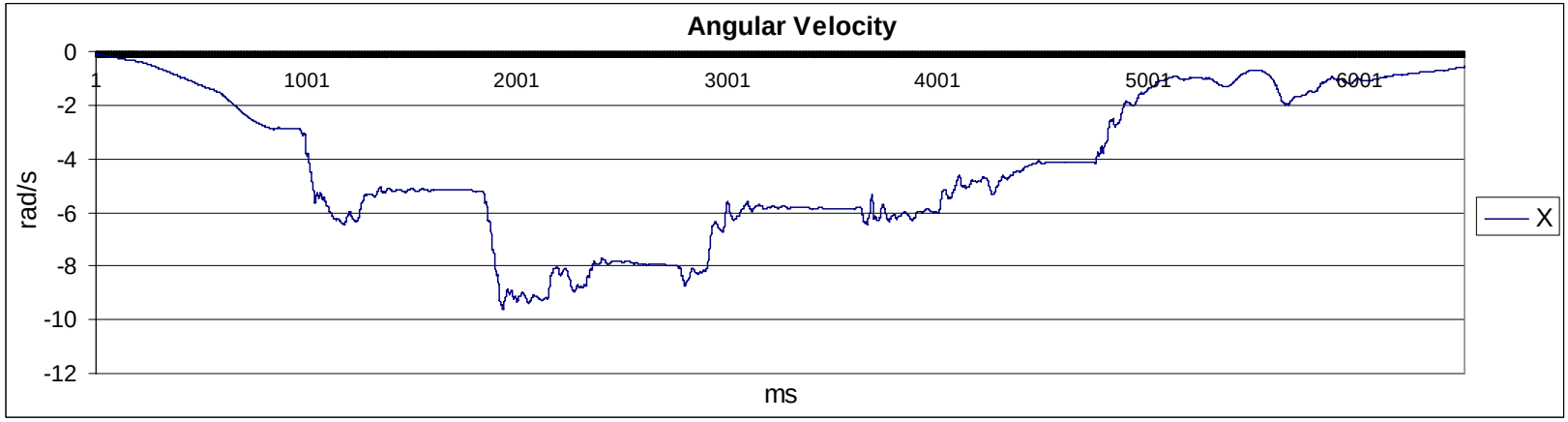

Appendix C

Pontiac Accelerometer Data

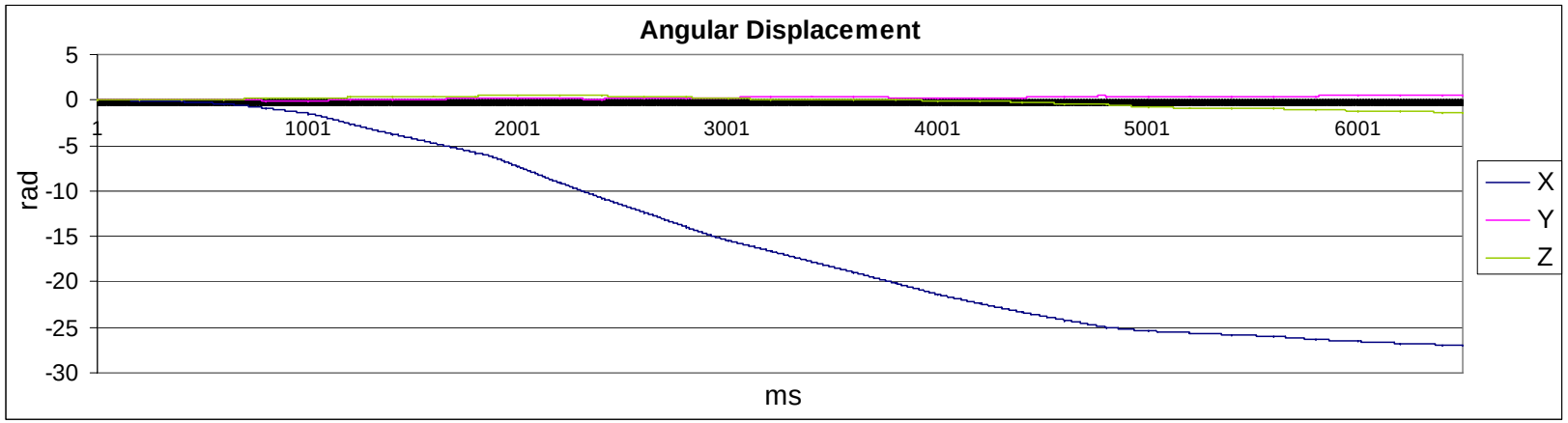

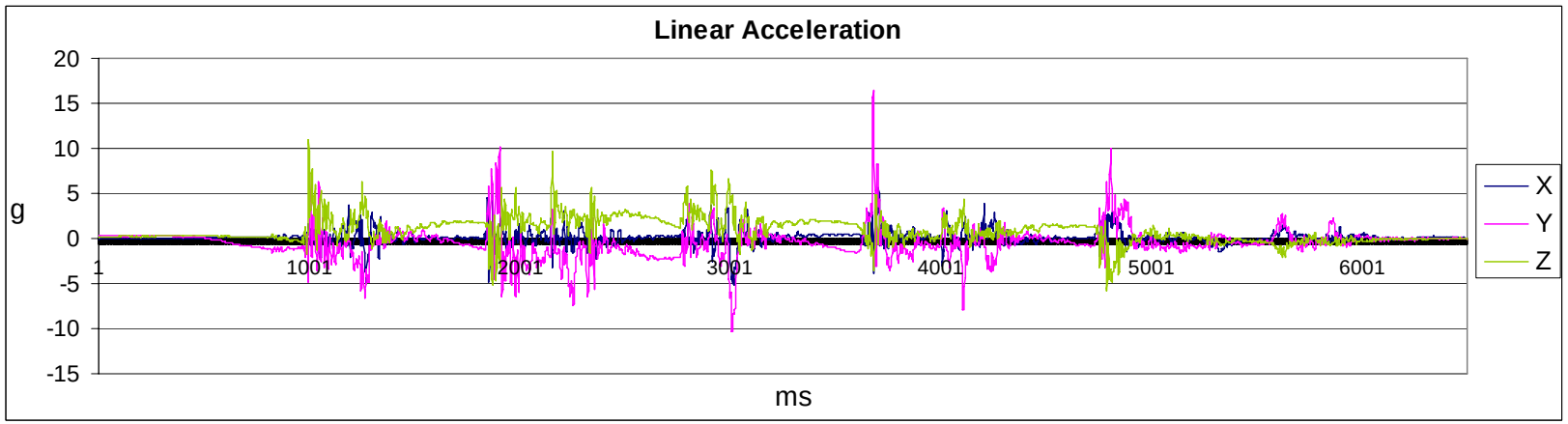

Appendix C

Pontiac Accelerometer Data